Eurasian Journal of Physics and Functional Materials

Manuscript 1259

Study of the Hole Behavior Properties of ITO/ZnO/VOPc/MoO3 /Al Devices by Varying the Temperature and Thickness via Impedance Spectroscopy

Madhusudhana Ramanna

Roopadevi Puttaswamy

Ramya Puttegowda

Sachin Shivakumar

Vinaykumar Linganna

See next page for additional authors

Study of the Hole Behavior Properties of ITO/ZnO/VOPc/MoO3 /Al Devices by Varying the Temperature and Thickness via Impedance Spectroscopy

Authors

Madhusudhana Ramanna, Roopadevi Puttaswamy, Ramya Puttegowda, Sachin Shivakumar, Vinaykumar Linganna, Ravikiran Ravikiran, Sachin Bandadka, and Guddappa Halligudra

ORIGINAL STUDY

Study of the Hole Behavior Properties of ITO/ZnO/VOPc/MoO_3/Al Devices by Varying the Temperature and Thickness via Impedance Spectroscopy

Madhusudhana Ramanna [a,*], Roopadevi Puttaswamy [b], Ramya Puttegowda [c], Sachin Shivakumar [d], Vinaykumar Linganna [e], Ravikiran [f], Sachin Bandadka [f], Guddappa Halligudra [g,**]

[a] Department of Physics, ATME College of Engineering, Mysuru, 570028, Karnataka, India
[b] Department of Physics, Government First Grade College for Women, Chamarajanagar, 571313, Karnataka, India
[c] Department of Physics, RV College of Engineering, Bengaluru, 560059, Karnataka, India
[d] Department of Physics, Maharaja Institute of Technology, Thandavapura, Nanjangud, Mysuru, 571302, Karnataka, India
[e] Department of Physics, JSS College of Arts, Commerce & Science (Autonomous), Mysuru, 570025, Karnataka, India
[f] Department of Mechanical Engineering, The National Institute of Engineering (NIE), Mysuru, 570008, Karnataka, India
[g] Department of Chemistry, ATME College of Engineering, Mysuru, 570028, Karnataka, India

Abstract

DC and AC electrical characteristics of vanadyl phthalocyanine thin films were arranged in an ITO/MoO_3/VOPc/MoO_3/Al sandwiched structure. By changing the thickness of the VOPc film within the range of 50−400 nm, the electrical properties of the fabricated diode device were examined at different temperatures. Analysis of real and imaginary components revealed insights into the resistance of the film and provided valuable information on the relaxation time. Notably, Cole−Cole plots demonstrated a correlation between film thickness and enhanced mobility, indicating an increase in film mobility with increasing thickness. This study determined the primary electrical conduction mechanism as a space charge-limited current with an exponential trap distribution. There was a remarkable increase in hole mobility, increasing from 8.25 × 10^{-9} $cm^2V^{-1}s^{-1}$ to 1.32 × 10^{-6} $cm^2V^{-1}s^{-1}$, corresponding to variations in the VOPc film thickness from 50 nm to 400 nm. Hole mobility was found to increase with increasing temperature, which was attributed to the increased injection of thermally generated charge carriers, along with a reduction in the barrier height.

Keywords: Impedance spectroscopy, Hole transport properties, Organic semiconductor devices, Vanadyl phthalocyanine thin films, Temperature-dependent electrical behavior, Space charge-limited conduction

1. Introduction

Metal phthalocyanines (MPcs), a class of organic semiconductors, have been widely studied for optoelectronic applications such as organic light-emitting diodes (OLEDs), organic solar cells (OSCs), and organic field-effect transistors (OFETs) owing to their stability, cost-effectiveness, and favorable charge transport properties [1−7]. Beyond these applications, MPcs have also shown potential in resistive random-access memory (ReRAM) and other non-volatile memory technologies, which are critical for next-generation data storage [8,9]. However, despite extensive exploration of planar phthalocyanines such as copper phthalocyanine (CuPc) for memory devices, investigations on non-planar phthalocyanines remain

Received 7 August 2025; revised 4 September 2025; accepted 16 September 2025.
Available online 20 November 2025

* Corresponding author.
** Corresponding author.
E-mail addresses: madhu84nano@gmail.com (M. Ramanna), hguddappa.m@gmail.com (G. Halligudra).

https://doi.org/10.69912/2616-8537.1259

limited [10−14]. Vanadyl phthalocyanine (VOPc), a non-planar MPc, offers distinct molecular geometry and superior electronic properties compared with planar counterparts [15−19]. These characteristics suggest that VOPc could be particularly advantageous for charge transport and resistive switching applications. Nevertheless, systematic studies on the temperature- and thickness-dependent electrical properties of VOPc thin films are scarce, and the fundamental conduction mechanisms governing these behaviors remain poorly understood [20−25]. Understanding these mechanisms is essential, as device performance in organic semiconductors is strongly influenced by film morphology, layer thickness, and interfacial energy alignment. In particular, hole transport and mobility are decisive parameters for optimizing the performance of devices such as OLEDs, photodiodes, and memory cells [26−29]. While impedance spectroscopy (IS) has been established as a powerful non-invasive tool to probe charge transport, dielectric relaxation, and carrier dynamics in organic semiconductors, its application to VOPc thin films in sandwiched device structures is still underexplored [30−34].

In this work, we systematically investigate the DC and AC electrical characteristics of VOPc thin films fabricated in an ITO/MoO_3/VOPc/MoO_3/Al layered structure. By varying the VOPc thickness from 50 to 400 nm and analyzing temperature-dependent impedance responses, we provide new insights into the relaxation dynamics, conduction mechanisms, and mobility enhancement in these films. Our results reveal that hole transport in VOPc follows a space charge-limited current (SCLC) mechanism with an exponential trap distribution, and we demonstrate a remarkable increase in hole mobility with increasing film thickness and temperature.

The novelty of this study lies in (i) the first detailed impedance spectroscopy analysis of VOPc thin films across varying thicknesses and temperatures, (ii) the identification of a clear correlation between thickness and enhanced hole mobility, and (iii) the experimental confirmation of SCLC as the dominant conduction mechanism in these systems. These findings not only expand the fundamental understanding of charge transport in non-planar MPcs but also highlight the potential of VOPc thin films for future applications in organic electronic and memory devices.

2. Materials and methods

The materials in this study were carefully selected based on their functional roles in device fabrication, including hole injection, hole transport, electron transport, and electrode characteristics. VOPc, MoO_3, and Al were used as received without further purification, while ZnO nanoparticles were synthesized in the laboratory.

2.1. Selection of transparent electrode

Glass substrates patterned with indium tin oxide (ITO) of 120 nm thickness and sheet resistance of 15 Ω were used. The work function of ITO varies between 4.4 and 4.9 eV depending on deposition and surface treatment. ITO functions as either an anode or a cathode within the device assembly, depending on the specific device configuration.

2.2. Hole injection material

MoO_3 was used as the hole injection material, which was procured from Sigma Aldrich with a purity of 99.98 % and was used for experimentation without any further purification. Its HOMO energy level, measuring 5.3 eV, matches nearly with the work function of both electrode materials, ITO and Al. Energy levels of both HOMO, LUMO, and work function of these materials are illustrated in the figure accompanying this description (Fig. 1).

2.3. Hole transport layer (VOPc)

Vanadyl phthalocyanine (VOPc) (Alfa Aesar) was used as the hole transport material because of its film-forming ability and favorable HOMO level (~5.4 eV). VoPc has been generally used in OLEDs and organic solar cells because of its favorable hole mobility value of 0.26 cm^2/V-s.

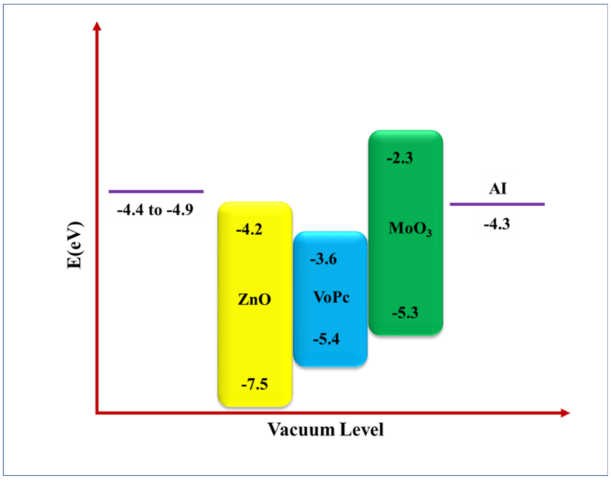

Fig. 1. HOMO LUMO energy levels of materials used for the fabrication of the device.

2.4. Cleaning of the ITO-coated glass substrate

Thoroughly cleaning the substrate is essential to ensure the proper functioning and reliability of the fabricated devices. Even a small amount of contamination on the ITO surface can alter its work function or the barrier height between the organic layer and the ITO, leading to unstable and unpredictable optical properties. To prepare the substrate, pre-patterned ITO-coated substrates featuring four ITO stripes with a 2 mm gap between them were initially mechanically washed with a chlorine solution, followed by rinsing with distilled water. These substrates subsequently undergo sequential ultrasonic cleaning in labolene, distilled water, acetone, and 2-propanol, with each step lasting approximately 20 min. After multiple ultrasonic rinses with distilled water, the substrates were dried with ultrapure nitrogen gas. Finally, the samples were degreased with acetone and vacuum dried at 100 °C for 10 min.

2.5. Electron transport material (ZnO NPs)

ZnO nanoparticles were synthesized via a green method using OM and GI plant extracts. Detailed procedures are reported in our earlier work [35].

2.6. Metal electrode (Al)

An aluminum film (Alfa Aesar, 99.9 % purity) was deposited as the top electrode matching the requirements for its specific function within the assembly.

2.7. Fabrication of device structure

The fabrication process involves three distinct types of devices: hole-only devices (ITO/MoO_3/VOPc/Al) to study hole transport, electron-only devices (ITO/ZnO/Al) to probe electron transport, and p-n junctions (ITO/MoO_3/VOPc/ZnO/Al) to study hybrid behavior. For hole-only devices, the aim was to investigate the hole transport properties within organic materials. These devices were assembled by placing a thin organic film between ITO and Al electrodes (Fig. 2). Additionally, to enhance the charge transport across the organic material, a thin layer facilitating hole injection was included in these structures. Further, electron-only devices have been specifically fabricated to study the electron transport properties of inorganic semiconductors. These devices also reveal the effect of changes in morphological structure and annealing temperature on the charge transport characteristics of these inorganic materials.

2.8. P-n junction

These devices comprise various layers, including inorganic and organic materials deposited on a glass substrate with a transparent electrode made of ITO, transmitting the penetration of visible light into the device. The device structure fabricated comprised multiple layers: an electron transport layer (ETL)/acceptor, a hole transport layer (HTL)/donor, and a hole injection layer (HIL) or/and electron-blocking layer (EBL). A metal electrode was placed on top of the device

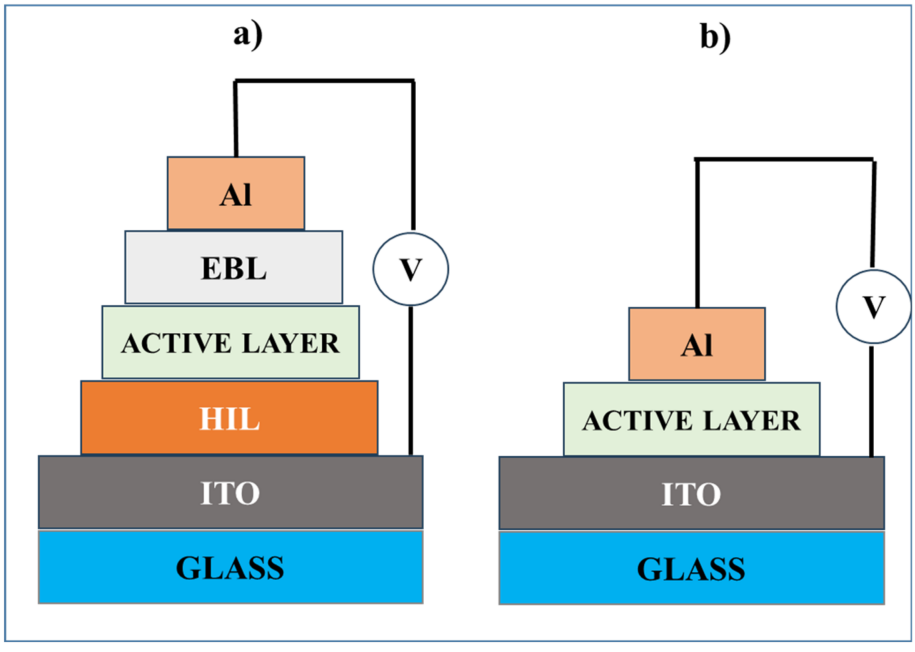

*Fig. 2. Schematic diagram of a hole-only device **(a)** and an electron-only device **(b)**.*

structure to serve as an anode to ensure continuity. This p-n junction set-up had MoO_3 as the HIL, VOPc as the HTL/donor, and ZnO as the ETL/acceptor (Fig. 3).

2.9. Preparation of ZnO NPs and its characterization

In this paper, we have fabricated a device structure with a layered deposition on an ITO-assisted glass substrate, upon which ZnO Nanoparticles were used. ZnO structures used in this device fabrication were synthesized in-house in the previously published data, and the same material is used in present work. ZnO Nanoparticles were synthesized via the green route method using OM and GI plant extract in aqueous media. The synthesized method of ZnO nanoparticles ensured a safe and green technique, which is eco-friendly and used in a wide variety of applications. A detailed synthesis procedure for the same, with their characterization results, is discussed in the paper. The XRD plots reported the crystallite sizes of 12.76 nm for OM-ZnO and 14.11 nm for GI-ZnO and exhibited a wurtzite structure. SEM pictographs confirmed the presence of ZnO nanoparticles, which were accumulated at various points and showed significant agglomeration with irregular spherical shape. The FT-IR spectral analysis proved the confirmation of Zn−O bond with a stretching at 480 cm-1 and confirmed the presence of different functional groups. UV-Vis Spectrophotometer revealed the peak absorption at 371 nm.

2.10. MoO_3 nanoparticles

In this paper, MoO_3 nanoparticles were fabricated onto the device structure with a layered deposition upon ZnO layer. These MoO_3 nanoparticles were procured from Adnano Technologies Company, India, and used directly for experimentation without any further purification.

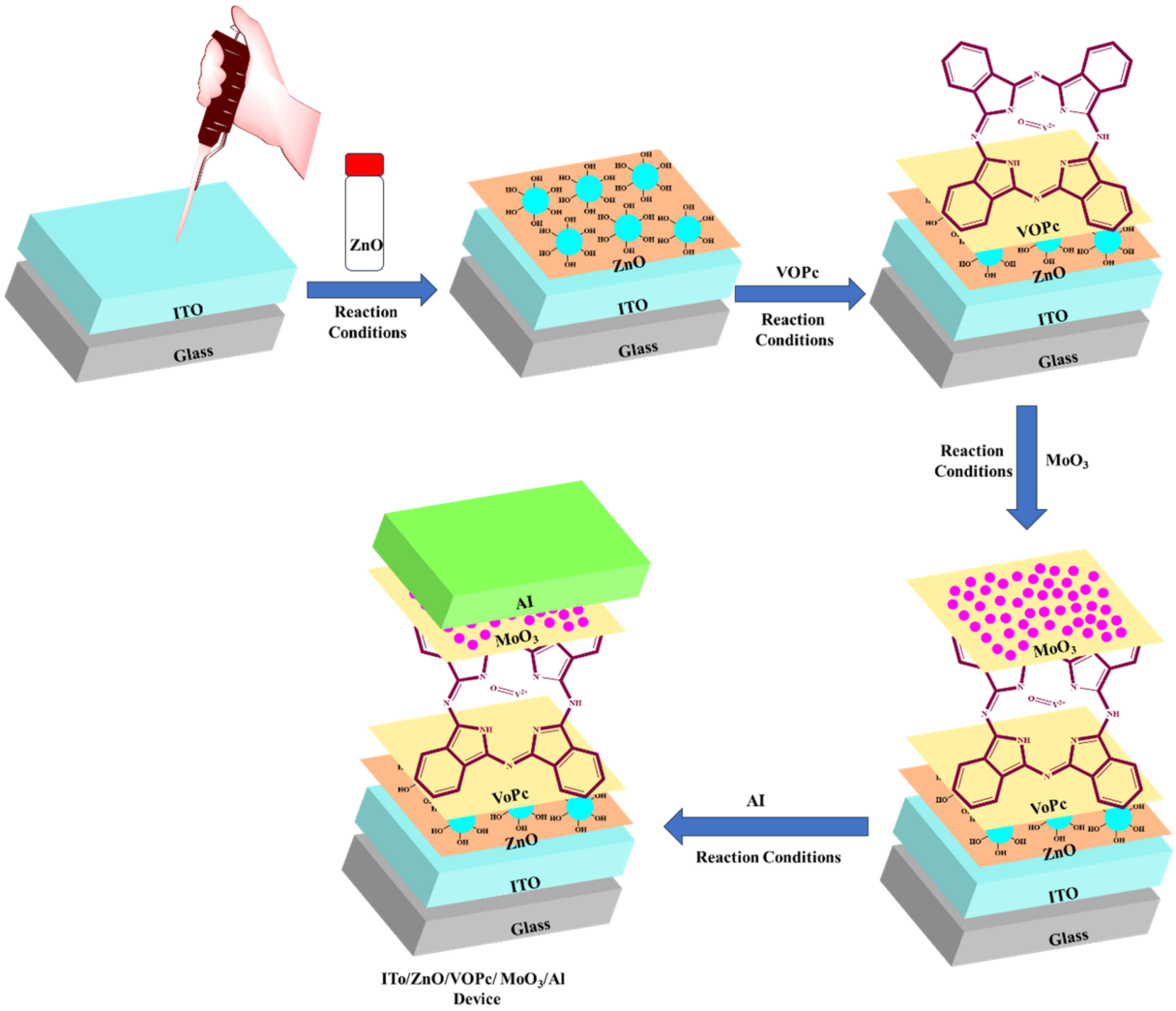

Fig. 3. Multi-layered deposition of various structures for device fabrication.

3. Results and discussion

3.1. Structural properties of ZnO nanoparticles

XRD analysis confirmed that the synthesized ZnO nanoparticles exhibited a wurtzite hexagonal structure. The average crystallite sizes were calculated to be 12.76 nm (OM-ZnO) and 14.11 nm (GI-ZnO).

3.2. Energy level alignment of MoO_3

The energy levels of MoO_3 were found to lie within the range of 2.3−5.3 eV, which is consistent with literature values. The introduction of a thin MoO_3 layer increased the effective work function of both ITO and Al electrodes, thereby improving hole injection into VOPc layers. This adjustment facilitates ohmic contact and reduces the injection barrier, which is critical for efficient charge carrier transport.

3.3. Impedance spectroscopy and electrical properties

Impedance spectroscopy (IS) was employed to study charge transport in the fabricated devices. The real and imaginary components of impedance revealed distinct relaxation features depending on film thickness and temperature. Cole−Cole plots showed that with increasing VOPc film thickness, there was a notable reduction in resistance and an enhancement in mobility, confirming improved charge transport pathways.

As the temperature increased, the peak frequency shifted toward higher values, indicating enhanced dielectric relaxation and thermally activated charge carrier mobility. A frequency-independent plateau was observed at low frequencies ($<10^3$ Hz), extending to higher frequencies with temperature, confirming a hopping conduction mechanism.

The conduction process was identified as space charge-limited current (SCLC) with an exponential trap distribution. Hole mobility increased significantly from 8.25×10^{-9} $cm^2V^{-1}s^{-1}$ (50 nm) to 1.32×10^{-6} $cm^2V^{-1}s^{-1}$ (400 nm). This mobility enhancement with both thickness and temperature was attributed to improved film morphology, reduced barrier height, and increased injection of thermally generated carriers. A non-invasive technique to determine and probe the frequency-dependent behavior of charge transport in devices is by impedance spectroscopy (IS). It gives important information on various parameters, including semiconductor interface, defect density, mobility, charge injections, electrode quality, and other elements that affect charge transport. Impedance spectroscopy measurements were carried out to study the electrical characteristics of the fabricated devices, particularly their charge transport behavior and injection mechanisms, by varying their temperature and thickness. Impedance spectroscopy provides information about the conduction mechanism, taking into account charge hopping conduction akin to dipole rotation.

The Z(f), i.e., complex impedance of the device, is given by

$$Z(f) = R(f) + iX(f) \quad (1)$$

where R(f) (or R) denotes resistance (the real part of the impedance) and X(f) (or X) indicates the capacitive reactance (the complex part of the impedance) (Fig. 4).

Upon analysis, the real and imaginary parts of the impedance frequency characteristics signify dominant patterns pertaining to different layer thicknesses at various temperatures. It is evident from the plot that the peak frequency increases with an increase in temperature. This increase is observed due to the decrease in parallel resistance of the device as the temperature increases, indicating an increase in dielectric relaxation. Consequently, conductivity increases as the temperature increases, and this change is directly attributed to thermally activated charge carrier mobility. As the temperature gradually increases, the release of the trapped charge carriers occurs, leading to an increase in free carrier density and, consequently, increased conductivity. It was found that alternating current (AC) conductance is directly proportional to temperature and frequency. In a spectrum of temperatures, there arises a frequency-independent zone for frequencies less than 10^3 Hz, named with the terminology “plateau”. This plateau extends into higher-frequency regions as the temperature is increased, indicating that the conduction mechanism is activated by temperature, which is evident in the increased conductance below 10^3 Hz. This nature coincides with the hopping mechanism influencing conductivity, particularly linked to the same processes with notable prolonged relaxation times.

The peak maximum decreases and moves toward lower frequencies as the temperature is increased, indicating an induction of thermal relaxation. Other notable influences of this behavior could be attributed to the charge hopping mobility, where at higher temperatures, defects or impurities are influenced primarily by relaxation, in relation to electron or immobile species predominating at lower temperatures. Changes in the relaxation peaks within the imaginary component specify temperature-dependent relaxation times. Moreover, the impedance tends to decrease with increasing frequency until approximately 10^6 Hz, above which a stable impedance value

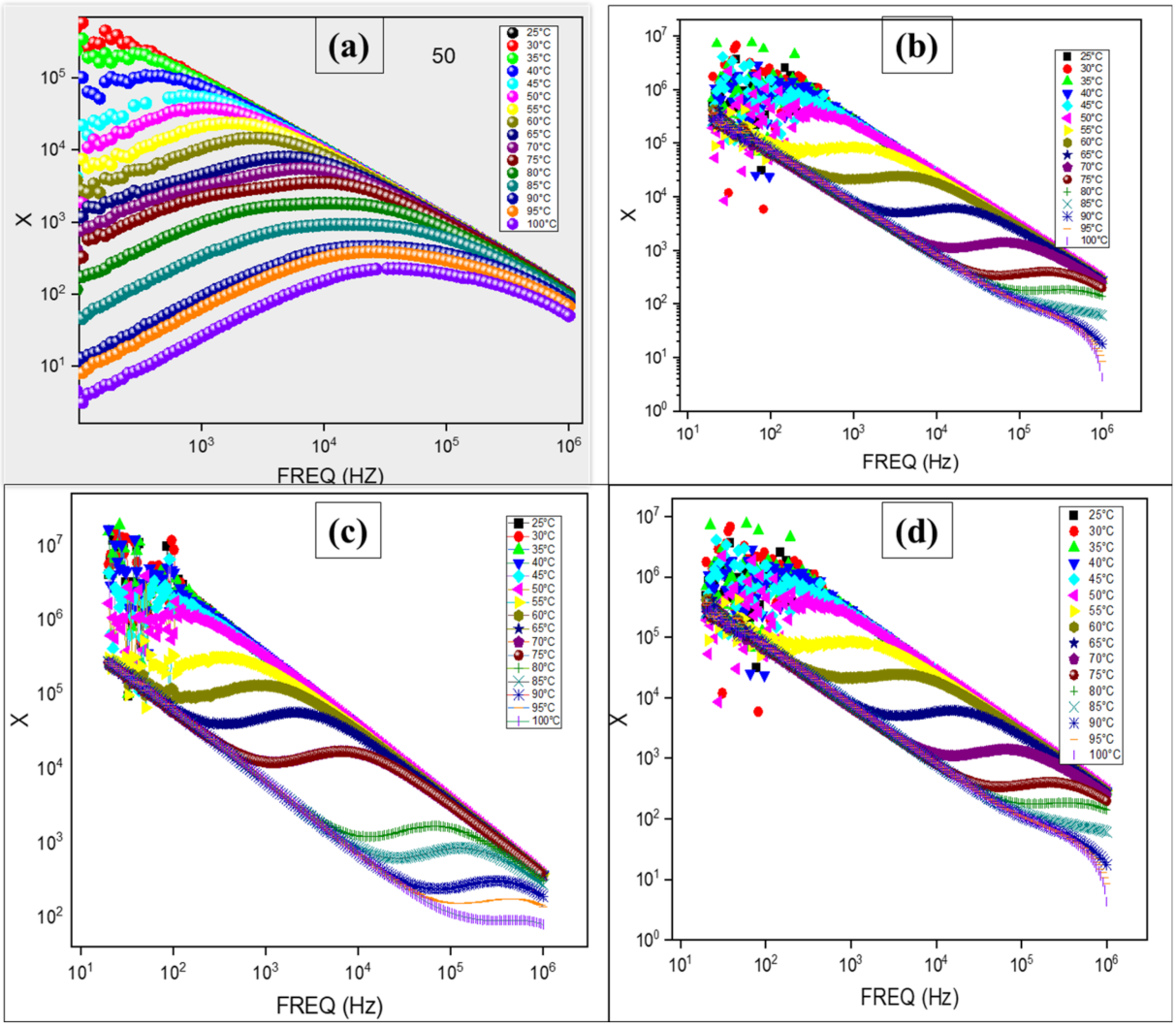

Fig. 4. Imaginary part of the impedance vs frequency plots for devices with ***(a)*** *50 nm,* ***(b)*** *100 nm,* ***(c)*** *200 nm and* ***(d)*** *400 nm VOPc layers.*

is achieved and becomes frequency-independent across a range of temperatures of study, which is consistent for both the imaginary and real impedance parts.

Examining the relationship between the real impedance and frequency across various temperatures reveals a decrease in impedance at lower frequencies as the temperature increases. However, at higher temperatures, the impedance begins to increase again. These differences are attributed to interactions between charge carriers and trapping centers coupled with thermal excitation. This variability likely arises from the increased AC conductivity with increasing temperature, resulting in improved carrier mobility, thereby decreasing the trap density and enhancing the charge carrier density. Variations in MoO_3 energy levels are influenced by surface state, material purity, thin film processing, and post-treatment techniques. Despite a notable discrepancy in the energy gap of approximately 3 eV, the current study designates energy band values within the range of 2.3–5.3 eV, as depicted in Fig. 5. The introduction of a thin MoO3 layer is known to enhance the work function of both ITO and Al electrodes, facilitating an ohmic connection between ITO and VOPc molecules.

Concerning the imaginary part of the impedance characteristics, with increasing frequency, X decreases consistently up to approximately 10^6 Hz, beyond which X values remain low and frequency independent across all investigated temperatures. This frequency-dependent conductivity is attributed primarily to the dominance of a hopping mechanism. Conductivity increases with an increase in frequency and is specifically associated with the electron hopping process, characterized by its significantly extensive relaxation time.

In Fig. 6, the mobility can be evaluated via the following formula:

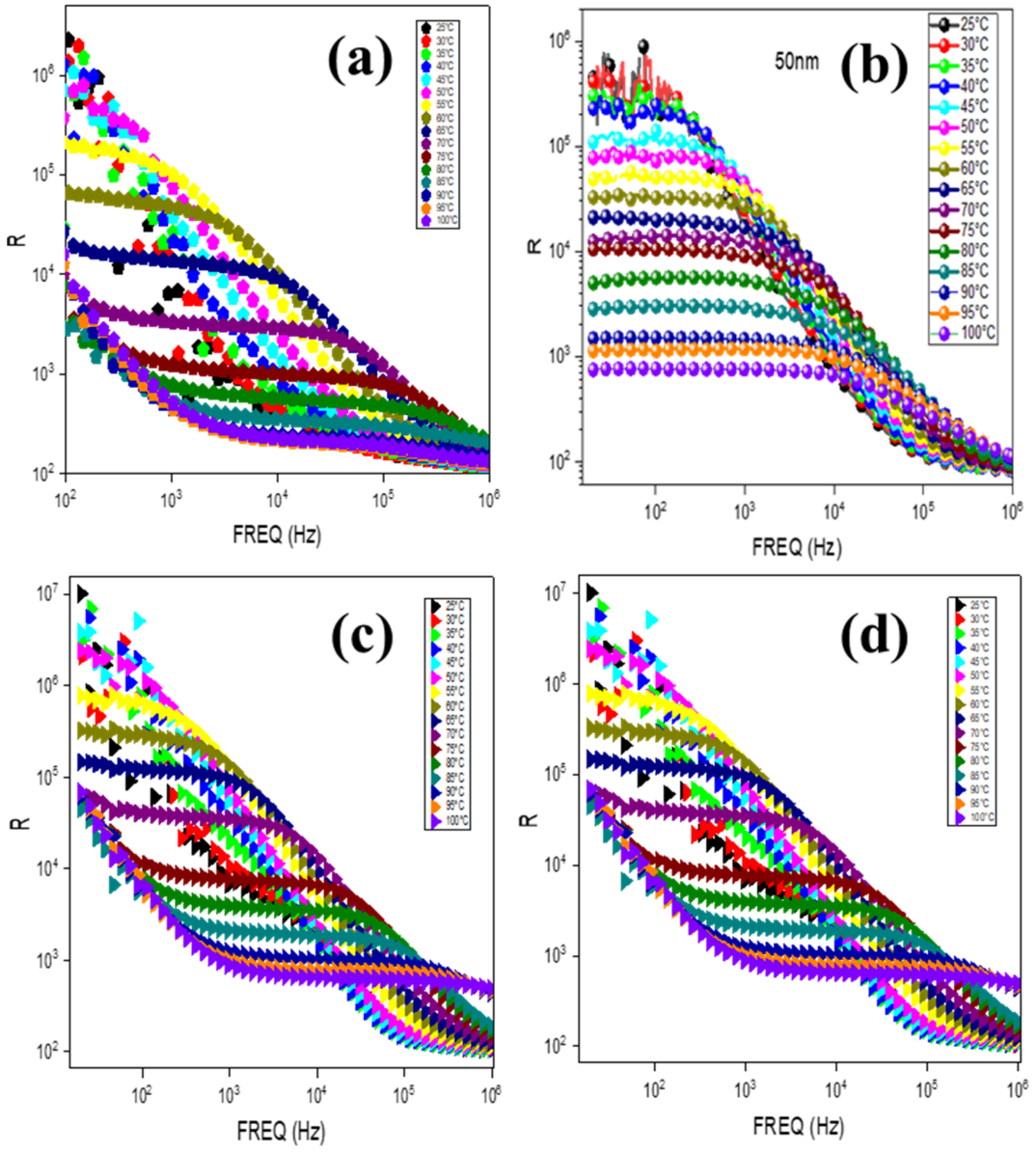

Fig. 5. Real part of the impedance vs frequency plots for devices with (a) 50 nm, (b) 100 nm, (c) 200 nm and (d) 400 nm VOPc layers.

$$\mu = \frac{qD}{K_B T} \tag{2}$$

$$D = \frac{L^2}{\tau_d} \tag{3}$$

Here, q denotes the electron charge, k_B is the Boltzmann constant, T indicates the absolute temperature, D is the diffusion coefficient, L denotes the thickness of the layer, and τ_d is the carrier transit time. As shown in Fig. 6, the results obtained from the plot of the mobility versus temperature display an increase in the mobility of the film with a tedious increase in the temperature, which specifies the efficiency of the device by increasing the electrical properties of the device.

3.4. Impedance analysis in frequency and complex plane

Figs. 4 and 5 illustrate the variation of imaginary (Z") and real (Z') parts of impedance as a function of frequency for devices with different VOPc layer thicknesses (50–400 nm) measured across the temperature range of 25–100 °C.

At lower frequencies, both Z' and Z" values are high, indicating strong electrode polarization and restricted charge carrier motion. As frequency increases, Z' and Z" gradually decrease, reflecting enhanced carrier dynamics and reduced polarization effects. The reduction in impedance with rising temperature suggests thermally activated charge transport and a lowering of potential barriers at the interfaces. While

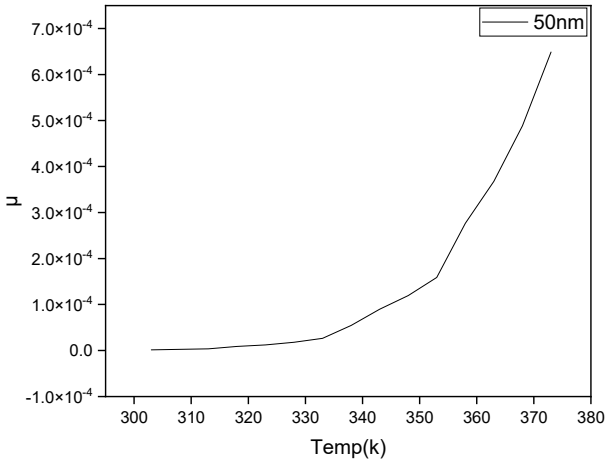

Fig. 6. Plot of mobility versus temperature for a film thickness of 50 nm.

frequency-dependent plots provide information on relaxation processes, further insight can be obtained by analyzing Z" as a function of Z' (Nyquist representation). In the complex impedance plane, semicircular arcs are typically observed, corresponding to bulk transport and interfacial phenomena. The diameter of these arcs decreases with increasing temperature, confirming the decrease in bulk resistance and the enhancement of conductivity. The appearance (or absence) of depressed semicircles provides additional evidence for non-Debye type relaxation and hopping conduction mechanisms.

Such Nyquist analysis, when fitted with an appropriate equivalent circuit model can yield quantitative parameters such as resistance, capacitance, and relaxation times, thereby deepening the understanding of conduction pathways and interface contributions in VOPc devices.

3.5. Temperature-dependent hole mobility

Fig. 6 shows the variation of mobility (μ) with temperature for the VOPc layer of 50 nm thickness. The extracted mobility corresponds to hole mobility (μh), since the studied configuration (ITO/MoO_3/VOPc/Al) is a hole-only device where current conduction is dominated by injected holes.

The mobility was calculated from impedance spectroscopy data using the SCLC model. The observed increase in μh with temperature indicates thermally activated transport typical of hopping conduction in disordered organic semiconductors. At lower temperatures, trap states limit charge movement, leading to suppressed mobility. As the temperature rises, carriers gain sufficient thermal energy to overcome trap barriers, resulting in enhanced hopping probability and hence increased mobility.

Such thermally activated hole transport confirms the dominance of the SCLC mechanism with an exponential trap distribution in VOPc thin films.

4. Conclusion

The particle size of ZnO nanoparticles was primarily estimated from XRD data using the Debye—Scherrer equation, which provided the crystallite size to be from 12 to 14 nm rather than the actual particle size. Although the exact particle size distribution was not obtained due to the absence of BET/zeta analysis, the crystallite size evolution trend aligns with the observed enhancement in device photo-response at an annealing temperature of 350 °C.

The films exhibited a polycrystalline nature with varying grain sizes and were subjected to detailed examination. In particular, hole-only devices utilizing VOPc as the active layer displayed notable chemical stability for up to 48 hours under ambient conditions, even without any protective encapsulation. When sol-gel spin-coated ZnO thin films prepared at different annealing temperatures were explored, it was observed that the nanoparticle size increased proportionally with increasing temperature. These nanoparticles exhibited a wurtzite hexagonal structure and maintained high transparency to visible light. Hybrid photodiodes developed using VOPc films in conjunction with ZnO nanoparticles revealed that devices utilizing ZnO films annealed at 350 °C exhibited superior photo-responses. This suggests the potential for organic-inorganic hybrid devices to function effectively as efficient photodiodes.

Data availability

No data were generated or analyzed during this study.

Consent for publication

All authors agree to publication.

Funding

We haven't received funding from any agency.

Conflict of interest

The authors declare that there are no conflicts of interest.

Acknowledgments

The authors sincerely thank ATME College of Engineering, Mysuru, for their support.

References

[1] G. Williams, S. Sutty, R. Klenkler, H. Aziz, Renewed interest in metal phthalocyanine donors for small molecule organic solar cells, Sol. Energy Mater. Sol. Cells 124 (2014) 217−226, https://doi.org/10.1016/j.solmat.2014.02.013.

[2] P.-C. Kao, S.-Y. Chu, Z.-X. You, S.J. Liou, C.-A. Chuang, Improved efficiency of organic light-emitting diodes using CoPc buffer layer, Thin Solid Films 498 (2006) 249−253, https://doi.org/10.1016/j.tsf.2005.07.120.

[3] O.A. Melville, T.M. Grant, B.H. Lessard, Silicon phthalocyanines as N-type semiconductors in organic thin film transistors, J. Mater. Chem. C 6 (2018) 5482−5488, https://doi.org/10.1039/C8TC01116H.

[4] H. Wang, D. Song, J. Yang, B. Yu, Y. Geng, D. Yan, High mobility vanadyl-phthalocyanine polycrystalline films for organic field-effect transistors, Appl. Phys. Lett. 90 (2007) 253510, https://doi.org/10.1063/1.2751103.

[5] N.A. Azarova, J.W. Owen, C.A. McLellan, M.A. Grimminger, E.K. Chapman, J.E. Anthony, O.D. Jurchescu, Fabrication of organic thin-film transistors by spray-deposition for low-cost, large-area electronics, Org. Electron. 11 (2010) 1960−1965.

[6] S.R. Forrest, The path to ubiquitous and low-cost organic electronic appliances on plastic, Nature 428 (2004) 911−918.

[7] A.N. Sokolov, M.E. Roberts, Z. Bao, Fabrication of low-cost electronic biosensors, Mater. Today 12 (2009) 12−20.

[8] Y.-H. Kim, J.E. Anthony, S.K. Park, Polymer blended small molecule organic field effect transistors with improved device-to-device uniformity and operational stability, Org. Electron. 13 (2012) 1152−1157, https://doi.org/10.1016/j.orgel.2012.03.016.

[9] K. Lian, R. Li, H. Wang, J. Zhang, D. Gamota, Printed flexible memory devices using copper phthalocyanine, Mater. Sci. Eng. B 167 (2010) 12−16, https://doi.org/10.1016/j.mseb.2010.01.020.

[10] X. Guo, J. Liu, L. Cao, Q. Liang, S. Lei, Nonvolatile memory device based on copper polyphthalocyanine thin films, ACS Omega 4 (2019) 10419−10423, https://doi.org/10.1021/acsomega.9b01224.

[11] S. Gao, X. Yi, J. Shang, G. Liu, R.-W. Li, Organic and hybrid resistive switching materials and devices, Chem. Soc. Rev. 48 (2019) 1531−1565, https://doi.org/10.1039/C8CS00614H.

[12] Y. Sun, D. Wen, X. Bai, Nonvolatile ternary resistive switching memory devices based on the polymer composites containing zinc oxide nanoparticles, Phys. Chem. Chem. Phys. 20 (2018) 5771−5779, https://doi.org/10.1039/C7CP07887K.

[13] Y. Shan, Z. Lyu, X. Guan, A. Younis, G. Yuan, J. Wang, S. Li, T. Wu, Solutionprocessed resistive switching memory devices based on hybrid organic−inorganic materials and composites, Phys. Chem. Chem. Phys. 20 (2018) 23837−23846, https://doi.org/10.1039/C8CP03945C.

[14] N. Raeis-Hosseini, J.-S. Lee, Resistive switching memory using biomaterials, J. Electroceram. 39 (2017) 223−238, https://doi.org/10.1007/s10832-017-0104-z.

[15] C. Wang, P. Gu, B. Hu, Q. Zhang, Recent progress in organic resistance memory with small molecules and inorganic−organic hybrid polymers as active elements, J. Mater. Chem. C 3 (2015) 10055−10065, https://doi.org/10.1039/C5TC02080H.

[16] S. Kim, S. Choi, W. Lu, Comprehensive physical model of dynamic resistive switching in an oxide memristor, ACS Nano 8 (2014) 2369−2376, https://doi.org/10.1021/nn405827t.

[17] D.S. Jeong, R. Thomas, R.S. Katiyar, J.F. Scott, H. Kohlstedt, A. Petraru, C.S. Hwang, Emerging memories: resistive switching mechanisms and current status, Rep. Prog. Phys. 75 (2012) 076502, https://doi.org/10.1088/0034-4885/75/7/076502.

[18] T. Harada, I. Ohkubo, K. Tsubouchi, H. Kumigashira, T. Ohnishi, M. Lippmaa, Y. Matsumoto, H. Koinuma, M. Oshima, Trap-controlled space-charge-limited current mechanism in resistance switching at Al/Pr0.7Ca0.3MnO3 interface, Appl. Phys. Lett. 92 (2008) 222113, https://doi.org/10.1063/1.2938049.

[19] Y. Yang, W. Lu, Nanoscale resistive switching devices: mechanisms and modeling, Nanoscale 5 (2013) 10076−10092, https://doi.org/10.1039/C3NR03472K.

[20] S. Baranovski, Charge Transport in Disordered Solids with Applications in Electronics, John Wiley & Sons, 2006.

[21] Y. Xiao, L. Zhang, F. Peng, G.-B. Pan, Fabrication of a cobalt phthalocyanine freestanding film on an ionic liquid surface for memory device applications, RSC Adv. 8 (2018) 5344−5349, https://doi.org/10.1039/C7RA12953J.

[22] Z. Khozaee, L. Sosa-Vargas, A.N. Cammidge, M.J. Cook, A.K. Ray, Hybrid phthalocyanine/lead sulphide nanocomposite for bistable memory switches, Mater. Res. Express 2 (2015) 096305, https://doi.org/10.1088/2053-1591/2/9/096305.

[23] Q. Meng, X. He, Q. Mao, Y. Weng, J. Yang, D. Yan, H. Zhao, Filamentary resistance switching in phthalocyanine thin films observed by electroluminescence, Appl. Phys. Lett. 106 (2015) 173302, https://doi.org/10.1063/1.4919648.

[24] B. Mukherjee, Resistive switching and nonvolatile memory in TiO2/CuPc nanocomposite devices, J. Electron. Mater. 48 (2019) 2131−2136, https://doi.org/10.1007/s11664-018-06891-z.

[25] K. Onlaor, B. Tunhoo, P. Keeratithiwakorn, T. Thiwawong, J. Nukeaw, Electrical bistable properties of copper phthalocyanine at different deposition rates, Solid State Electron. 72 (2012) 60−66, https://doi.org/10.1016/j.sse.2012.01.003.

[26] S. Choi, S.-H. Hong, S.H. Cho, S. Park, S.-M. Park, O. Kim, M. Ree, High-performance programmable memory devices based on hyperbranched copper phthalocyanine polymer thin films, Adv. Mater. 20 (2008) 1766−1771, https://doi.org/10.1002/adma.200702147.

[27] Y. Pan, X. Liao, Y. Wu, L. Chen, You-yuan Zhao, Y. Shen, F. Li, S. Shen, D. Huang, Steady-state photovoltaic and electroreflective spectra in Al/vanadyl phthalocyanine (VOPc, in phase II)/indium−tin−oxide (ITO) sandwich cell, Thin Solid Films 324 (1998) 209−213, https://doi.org/10.1016/S0040-6090(98)00357-5.

[28] M.R. Kiran, H. Ulla, M.N. Satyanarayan, G. Umesh, Optoelectronic properties of hybrid diodes based on vanadyl-phthalocyanine and zinc oxide, Superlattices Microstruct 112 (2017) 654−664, https://doi.org/10.1016/j.spmi.2017.10.023.

[29] M.R. Kiran, H. Ulla, M.N. Satyanarayan, G. Umesh, Effect of deposition rate on the charge transport in vanadyl-phthalocyanine thin films, Synth. Met. 224 (2017) 63−71, https://doi.org/10.1016/j.synthmet.2016.12.025.

[30] M. Raveendra Kiran, H. Ulla, M.N. Satyanarayan, G. Umesh, Optoelectronic properties of hybrid diodes based on vanadyl-phthalocyanine and zinc oxide nanorods thin films, Opt. Mater. 96 (2019) 109348, https://doi.org/10.1016/j.optmat.2019.109348.

[31] N.T. Boileau, R. Cranston, B. Mirka, O.A. Melville, B.H. Lessard, Metal phthalocyanine organic thin-film transistors: changes in electrical performance and stability in response to temperature and environment, RSC Adv. 9 (2019) 21478−21485, https://doi.org/10.1039/C9RA03648B.

[32] B. Ebenhoch, N.B.A. Prasetya, V.M. Rotello, G. Cooke, I.D.W. Samuel, Solution processed boron sub phthalocyanine derivatives as acceptors for organic bulk-heterojunction solar cells, J. Mater. Chem. A 3 (2015) 7345−7352, https://doi.org/10.1039/C5TA00715A.

[33] H. Chan, H.-L. Wong, M. Ng, C.-T. Poon, V.W.-W. Yam, Switching of resistive memory behavior from binary to ternary logic via alteration of substituent positioning on the subphthalocyanine core, J. Am. Chem. Soc. 139 (2017) 7256−7263, https://doi.org/10.1021/jacs.7b00895.

[34] Novel thermally stable single-component organic-memory cell based on oxo-titanium phthalocyanine material, IEEE Electron Device Lett. 30 (2009) 931−933, https://doi.org/10.1109/LED.2009.2025893.

[35] G. Halligudra, J. L.S.K., V. K, et al., Antibacterial and Antiproliferative effect of ZnO nanoparticles prepared using origanum marjorana plant and Garcinia indica Fruit extracts, J Inorg Organomet Polym 35 (2025) 1073−1083, https://doi.org/10.1007/s10904-024-03349-0.